Chapter 4

The Uranium-Oxygen system

The complexity of the uranium-oxygen system is responsible for many of the problems encountered when considering it experimentally or theoretically. Even the seemingly simple UO_2 system exhibits a wide range of experimentally obtained diffusion coefficients for some fission products. Most of these experimental problems are a result of stoichiometry changes during the experiment. Figure 4.1 shows the phase diagram of the UO_2 system [8, 9].

As stated before, we are interested in the high temperature phases of the uranium-oxygen system. When oxidising UO_2 at high temperature, the results include mixed phases of U_3O_8 and UO_2. Below 1400 K the U_4O_9 phase is also present in the oxidation sequence.

4.1 UO_2

Extensive experimental studies on UO_2 have been performed ever since the ceramic was first used in nuclear reactors. The first (confidential) reports on fission product migration are dated as early as 1941, even before Enrico Fermi's CP-1 reactor

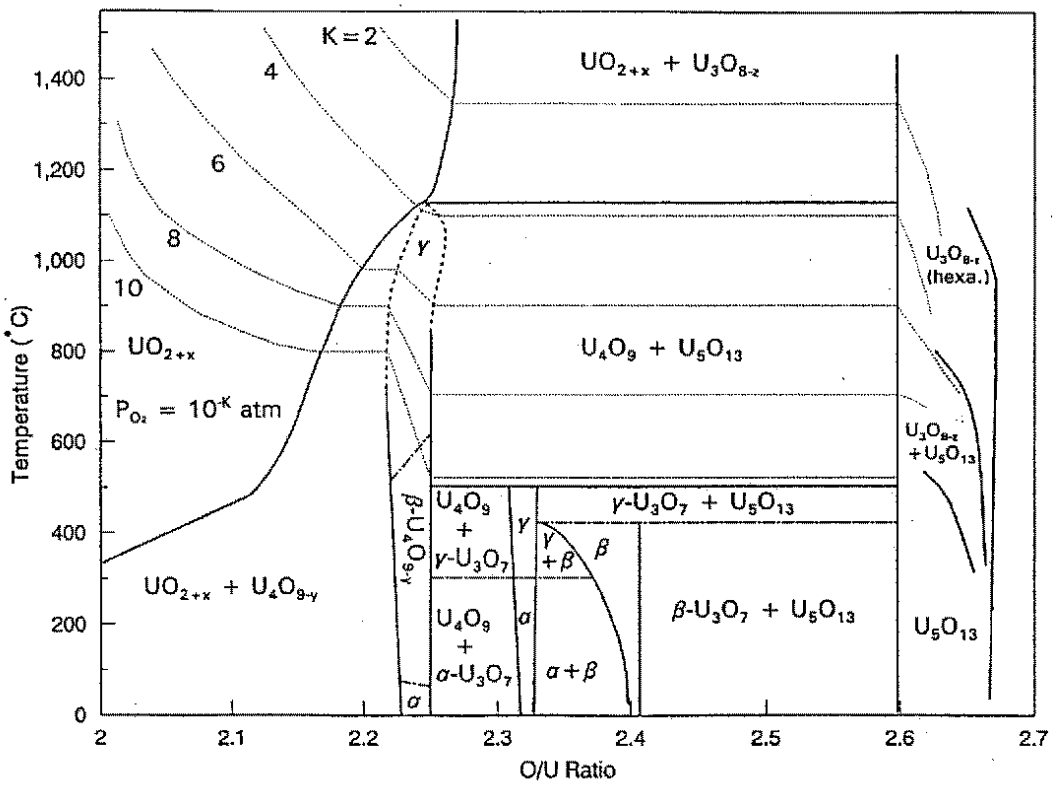

Figure 4.1: Uranium-Oxygen phase diagram taken from Naito *et al.* [8] and Bradford [9].

had demonstrated the possibility of nuclear fission. Early experimental and theoretical work centered around the nuclear properties of uranium and plutonium (e.g. "Nuclear Fission" [13]).

When early fission reactor designs were considered, fission product migration and chemical issues such as the fuel oxide potential and the effect of various container metals on the fuel became important. The chemistry of the fuel-cladding gap is an important part of nuclear fuel design.

In this study we are interested in the state of the fuel after irradiation. As

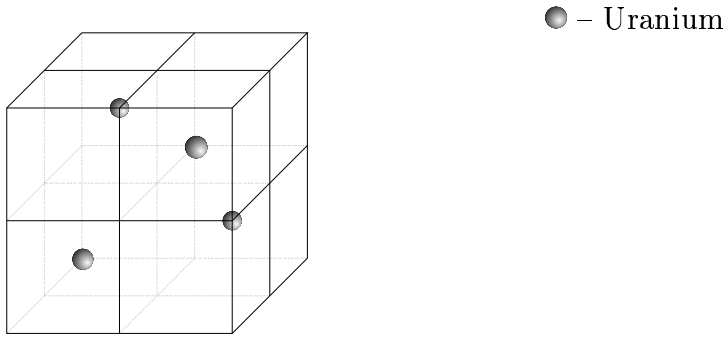

Figure 4.2: UO_2 adopts the fluorite structure. Oxygen atoms occupy the corners of the cubes.

mentioned in the introduction, the fuel undergoes various changes during its active life. The accumulation of fission products in the fuel matrix and the occurrence of radiation damage in the form of intrinsic type defects and large scale defects such as vacancy clusters and large voids all influence the migration of fission products. Furthermore the stoichiometry of the fuel can change when the cladding fails and the fuel comes into contact with an oxidising atmosphere.

4.1.1 Materials properties

UO_2 adopts the face-centered-cubic fluorite structure (space group $Fm3m$, No. 225), shown in Figure 4.2.

A summary of UO_2 materials properties can be found in Table 4.1. The elastic constants have been determined by crystallographic methods [54] and are used in the derivation of inter-atomic potentials. The lattice energy was determined by a Born-Harber cycle experiment, where a crystal is melted, evaporated and the gas molecules are ultimately dissociated. The energy of the thermodynamic cycle is then derived by carefully considering the heats of melting, evaporation and dissociation.

Data on the UO_2 phase.			
Property	Symbol	Value	
Structure		Fluorite	
Lattice Parameter	a	5.468 Å	
Elastic constants	C_{11}	396 GN/m^2	Fritz 1976 [54]
	C_{12}	121 GN/m^2	
	C_{44}	61 GN/m^2	
Dielectric constants	ϵ^0	24.0 ϵ	Schoenes and Hampton [55, 56]
	ϵ^∞	5.30 ϵ	
Band gap		2.3 eV	[57]
Ionization potentials			
$U \rightarrow U^+$		5.54 eV	[58]
$U^+ \rightarrow U^{2+}$		10.39 eV	
$U^{2+} \rightarrow U^{3+}$		18.44 eV	
$U^{3+} \rightarrow U^{4+}$		31.06 eV	
$U^{4+} \rightarrow U^{5+}$		45.77 eV	
$U^{5+} \rightarrow U^{6+}$		61.07 eV	
Lattice energy	H_L	-106.7 eV	[59]
Oxygen Frenkel enthalpy	E_F^O	3.0-4.0 eV	[60]
Uranium Frenkel enthalpy	E_F^U	9.5 eV	
Schottky energy	E_S	6-7 eV	

Table 4.1: Data on the UO_2 phase.

Self-diffusion data			
Lattice	D_0 [m^2s^{-1}]	ΔH_A [eV]	Ref.
Oxygen:			
UO_{2-x}	$2.2 \times 10^{-8}\|x\|$	0.51	[61]
UO_2	2.6×10^{-5}	2.6	[61]
UO_{2+x}	$2.5 \times 10^{-7}x$	0.91	[62, 63]
Uranium:			
UO_{2-x}		5-7.8	[64]
UO_2	6.5×10^{-5}	5.6	[64]
UO_{2+x}		2.6	[64]
U_3O_8		2.4	[48]

Table 4.2: The self diffusion of intrinsic defects in $UO_{2\pm x}$ and U_3O_8.

Ionization energies of uranium [58] and electron affinities of oxygen must also be considered. The electron affinity is based upon the 2.3 eV band gap measured by Bates *et al.* [57]. The enthalpies listed in Table 4.1 are important to us, because they are parameters in vacancy assisted diffusion mechanisms. The low oxygen Frenkel energy suggests that the Frenkel disorder is the dominant disorder process in UO_2.

4.1.2 Self diffusion and radiation enhanced diffusion

The thermal self diffusion data of uranium and oxygen in $UO_{2\pm x}$ are summarized in Table 4.2. Clearly the activation enthalpy for self diffusion of oxygen and uranium ions is highly dependent on the stoichiometry. The pre-exponential depends linearly on the extent of the non-stoichiometry, x.

There are secondary ion mass spectroscopy results by Sabioni [65] which suggest

a migration actication energy for uranium in UO_2 of 4.4 eV. This study shows some uncertainty regarding the actual stoichiometry of the material used as well as the stability of the stoichiometry during the experiment.

Under irradiation conditions, the diffusion of uranium ions is modified and the diffusion coefficient is linear with the neutron flux [66]:

$$D = 1.2 \times 10^{-29} F \quad [cm^2 s^{-1}], \tag{4.1}$$

where F is the fission rate in $f/cm^3 s$. The effects of radiation remain present after the fuel is taken out of the pile. Matzke suggests that the radiation damage effects on uranium diffusion can be annealed at 973-1173 K. The range of the uranium during annealing is not more than 3 nm.

4.1.3 Stoichiometry

The stoichiometry of the UO_2 lattice controls how defect processes in the fuel take place. Firstly the availability of oxygen vacancies and interstitials is controlled by the stoichiometry. This in turn controls the abundance of uranium vacancies and electronic defects, both of which are important to migration and defect processes.

In UO_{2+x} at lower temperatures ordering of interstitials can occur, which is the precursor to U_4O_9 formation through e.g. Willis clusters [67–69].

4.1.4 Fission products

Most experimental data to date are based on release experiments in a situation where the stoichiometry is controlled and the sample is annealed. It is understood that high temperature release is controlled by the transport of the fission products from the grains to the grain boundary. Diffusion through the grain boundary is believed

to be very fast, especially at high burn up, because of the formation of pores from large fission gas bubbles at grain boundaries [70] (Figure 4.3). Microscopy studies show the formation of channels through the boundaries.

Some fission products (especially gaseous Xe and Kr but in some conditions Cs and I) form bubbles [60]. Fission products can be released from bubbles by resolution and consecutive atomic diffusion or by bubble diffusion [71, 72]. Resolution can be radiation induced as well as thermal, so again there is a difference between in-pile and ex-pile diffusion of these fission products.

Caesium

The release of the fission product caesium from UO_2 has been studied by Prussin *et al.* [7] and by Akabori and Fukuda [74]. In both studies the material used was stoichiometric, polycrystalline UO_2 with a $10\mu m$ grain size. The data from Prussin *et al.* was treated using the Booth model (see Section 3.4.3) as described in Akabori and Fukuda [74] and plotted in Figure 4.4. The Arrhenius equations for the fits in Figure 4.4 are listed in Table 4.3. Both experiments agree on the activation enthalpy for migration, but the pre-exponential factors differ by two orders of magnitude. This is not unusual, as the absolute diffusion coefficient is difficult to measure experimentally, partly due to the uncertainty surrounding the a value in the Booth model (see Section 3.4.3).

Iodine

Results for post irradiation iodine diffusion by Prussin *et al.* contain some scatter and seem to suggest an activation enthalpy of 5.4±2.0 eV. Studies by Friskney and Turnbull [53] on iodine release during irradiation show clearly that under those

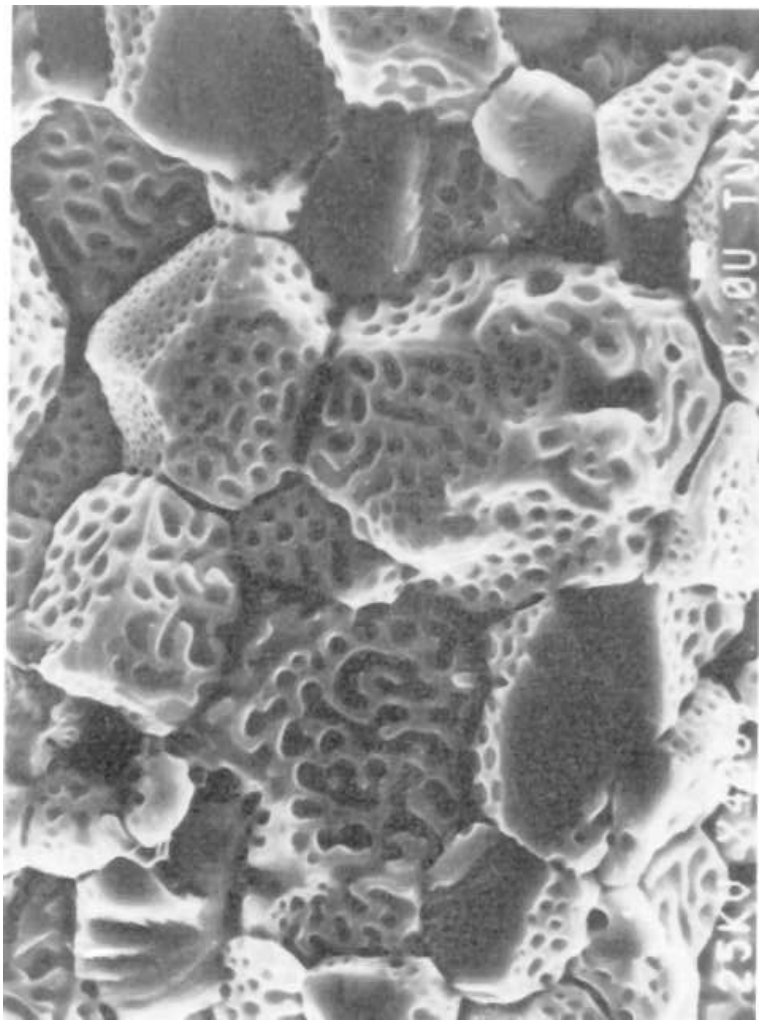

Figure 4.3: Formation of pores from large fission gas bubbles at the grain boundary, taken from Matzke, 1989 [73].

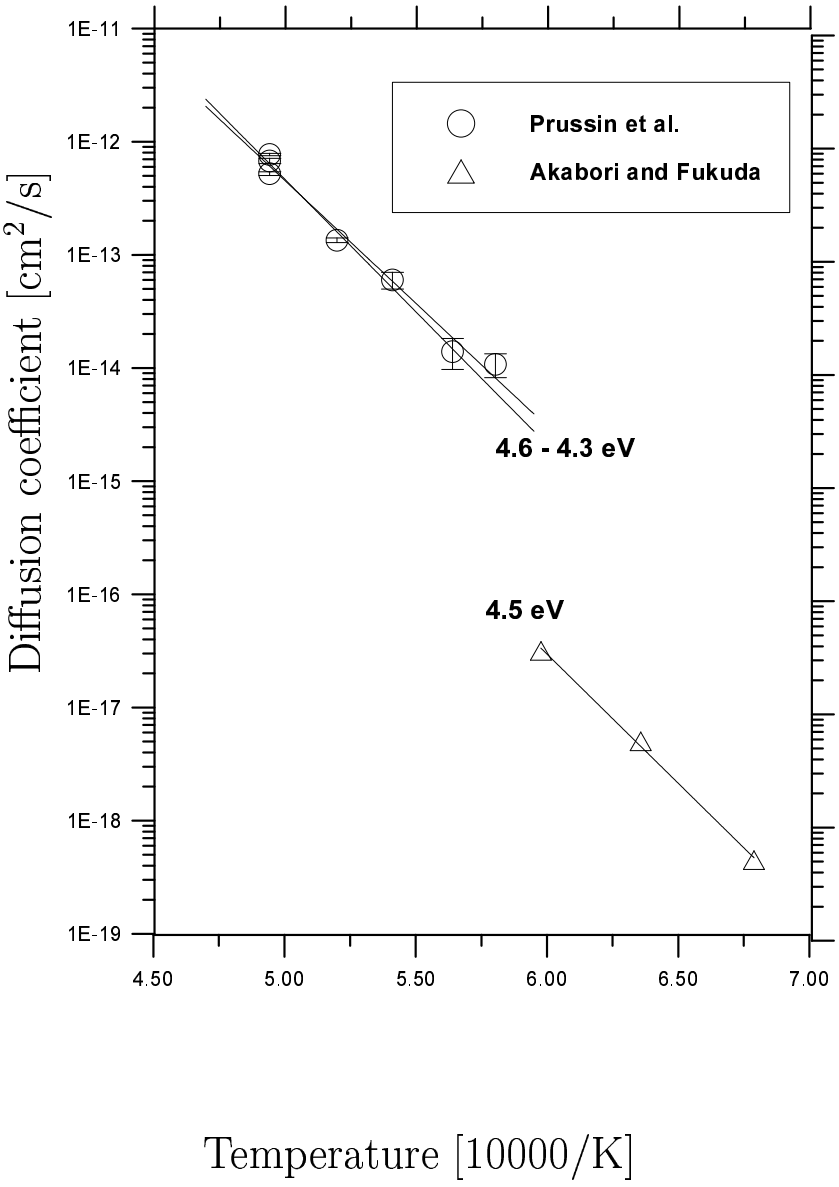

Figure 4.4: An Arrhenius plot of caesium data taken from Prussin *et al.* [7] and Akabori and Fukuda [74]. The activation enthalpies of the fits are indicated in the figure. Details of the fits are given in Table 4.3

Arrhenius equations for caesium diffusion		
1473-1673 K	$D(T) = 1.5 \times 10^{-3} \exp(4.5eV/kT)$ [cm^2/s]	[74]
1723-2023 K	$D(T) = 3.4 \times 10^{-2} \exp(4.3eV/kT)$ [cm^2/s]	[7]
1723-2023 K	$D(T) = 2.6 \times 10^{-1} \exp(4.6eV/kT)$ [cm^2/s]	[7]

Table 4.3: Predicted Arrhenius equations for Cs, data taken from refs. [7, 74]. The Arrhenius equations are plotted in Figure 4.4

conditions the activation enthalpy increases significantly at approximately 1300 K. The results of these two studies are shown in Figure 4.5. Arrhenius fits to the data are shown in Table 4.4.

The Arrhenius energies predicted by Friskney and Turnbull are much lower than those suggested by Prussin *et al.* . This is not surprising as the Friskney and Turnbull results were obtained from in-pile experiments, where radiation damage rather than thermal processes is responsible for the formation of intrinsic defects which assist the diffusion of fission products [66]. The low temperature process is *not* a result of atomic diffusion, because the pre-exponential factor is about 10 orders of magnitude smaller than would be expected for such a process (see Section 3.1 for a discussion on the magnitude of the pre-exponential).

According to Johnson *et al.* large increases in iodine release also occur when the UO_2 fuel is oxidised [75].

Other fission products

Initial fission product work concentrated on the gasseous sustances such as helium and xenon. Reliable ex-pile xenon diffusion coefficients were determined by Miekeley and Felix and later Prussin [7,76]. Both solution, migration and concentration effects

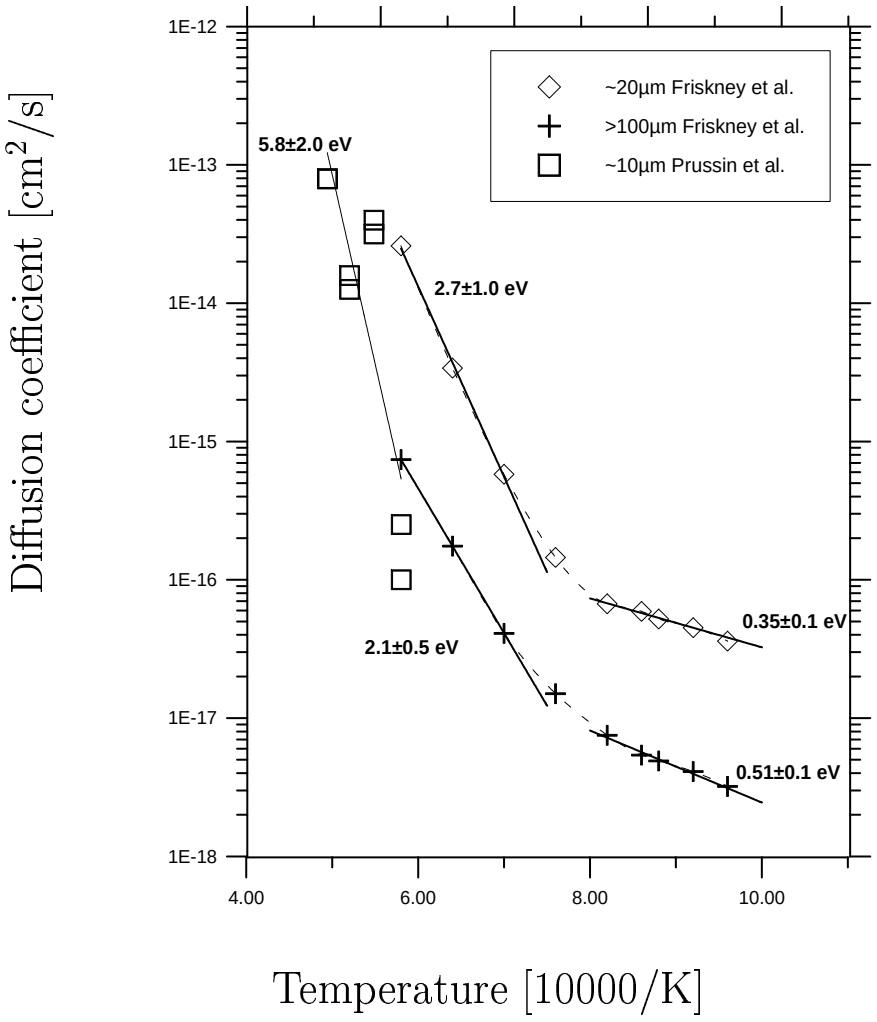

Figure 4.5: An Arrhenius plot of the diffusion coefficients of iodine in UO_2 according to Friskney *et al.* [53] and Prussin *et al.* [7] with some suggested activation energies. Details of the fits for the 10-20μm results are listed in Table 4.4

Arrhenius equations for iodine diffusion		
1050-1200 K	$D(T) = 1.9 \times 10^{-15} \exp(0.35eV/kT)$ [cm^2/s]	[53]
1300-1700 K	$D(T) = 2.4 \times 10^{-6} \exp(2.7eV/kT)$ [cm^2/s]	[53]
1700-2000 K	$D(T) = 4.3 \exp(5.4eV/kT)$ [cm^2/s]	[7]

Table 4.4: Predicted Arrhenius equations for I data taken from refs. [7, 53]. The fitted equations are plotted with the data in Figure 4.5.

of xenon in $UO_{2\pm x}$ have been studied with the atomistic simulation methodology in the past [77–80].

Ruthenium

Recently, there has been an increased interest in the behaviour of ruthenium under oxidizing conditions both in fuel and in waste repositories. With a half-life of 1.01 years, Ru-106 is a radiologically important fission product. In the Chernobyl accident ruthenium was considered to have been emitted at a similar rate as other volatile fission products [81, 82].

In UO_2 ruthenium is one of the metals that can precipitate in a metal cluster at high burn up [16], together with Mo, Pt, Pd and Te. To understand ruthenium release from nuclear fuel it is important to realise that these precipitates are often found at grain boundaries or in fission gas bubbles [18].

The fuel history, temperature and oxidizing conditions have a great impact on the way ruthenium may be released from UO_2 fuel. Two types of experiments are distinguishable in literature: post-irradiation analysis of fuel and controlled measurement of ruthenium migrating through UO_2 in a solution experiment.

In the latter experiment, it is likely that the measurements reflect the bulk diffusion coefficient. These results can easily be compared with the theoretical results presented in this thesis. Bulk diffusion is responsible for the formation of the metal particles (mostly at grain boundaries) during irradiation. Since this is an in-pile process, diffusion will be enhanced by the continuous formation of intrinsic defects by radiation (see Section 4.1.2).

Work by Yang [49] does not rely on release, but measures the penetration of RuO_2 into UO_2. Results by Whittingham *et al.* [83] do rely on the release of RuO_3 or RuO_4, but this is done under oxidising conditions where the oxidation of ruthenium is not likely to be a rate controlling step.

Observations on post-irradiation fuel clearly demonstrate that ruthenium is only

Arrhenius equations for ruthenium diffusion		
1020-1700 K	$D(T) = 0.3\exp(-2.1eV/kT)\ [a^2/s]$	(U_3O_8) [83]
1473-1973 K	$D(T) = 3.2 \times 10^{10}\exp(-6.7eV/kT)\ [a^2/s]$	(UO_2) [50]
1473-1973 K	$D(T) = 4.7 \times 10^{-5}\exp(-0.7eV/kT)\ [a^2/s]$	($UO_{2.2}$) [50]
2060-2300 K	$D(T) = 1.5 \times 10^{8}\exp(-8.2eV/kT)\ [cm^2/s]$	(UO_2) [49]

Table 4.5: Fits to data presented in Figure 4.6.

released once the fuel reaches stoichiometry. The release is highly temperature dependent in this case [84, 85]. Further oxidation stimulates ruthenium release and reduces the temperature dependence significantly.

Once the oxidation of the fuel reaches the point where U_3O_8 is formed, fuel oxidation no longer competes with RuO_3 or RuO_4 formation [83, 86, 87] and all metallic ruthenium is quickly released from the fuel via grain boundaries.

Although the release and diffusion of ruthenium is still not completely understood [88] some of the diffusion data may be explained with the currently available release models. Diffusion data taken from Yang 1980 [49], Prussin 1995 [50] and Whittingham 1996 [83] are shown in Figure 4.6. Fitted Arrhenius parameters are reported in Table 4.5.

The data by Whittingham shows a reasonable pre-exponential D_0 which may well be a result of bulk diffusion.

Both data sets by Prussin have D_0 values which are orders of magnitude larger and smaller than would be expected if bulk diffusion were the controlling mechanism. The high value for D_0 is more than likely an artifact of the surface oxidation reaction of metal particles occurring at low oxygen partial pressure near UO_2. The very low value for D_0 combined with a very low activation energy in $UO_{2.2}$ may well be the

result of fast oxidation and release of ruthenium through the grain boundary.

Results by Yang are not well understood, especially since the experiments performed are well controlled penetration experiments. Nevertheless, the pre-exponential is very high and can not be true bulk diffusion in UO_2. A possibility is that grain boundary diffusion plays some role here, yet if that were the case, a lower activation enthalpy would be expected.

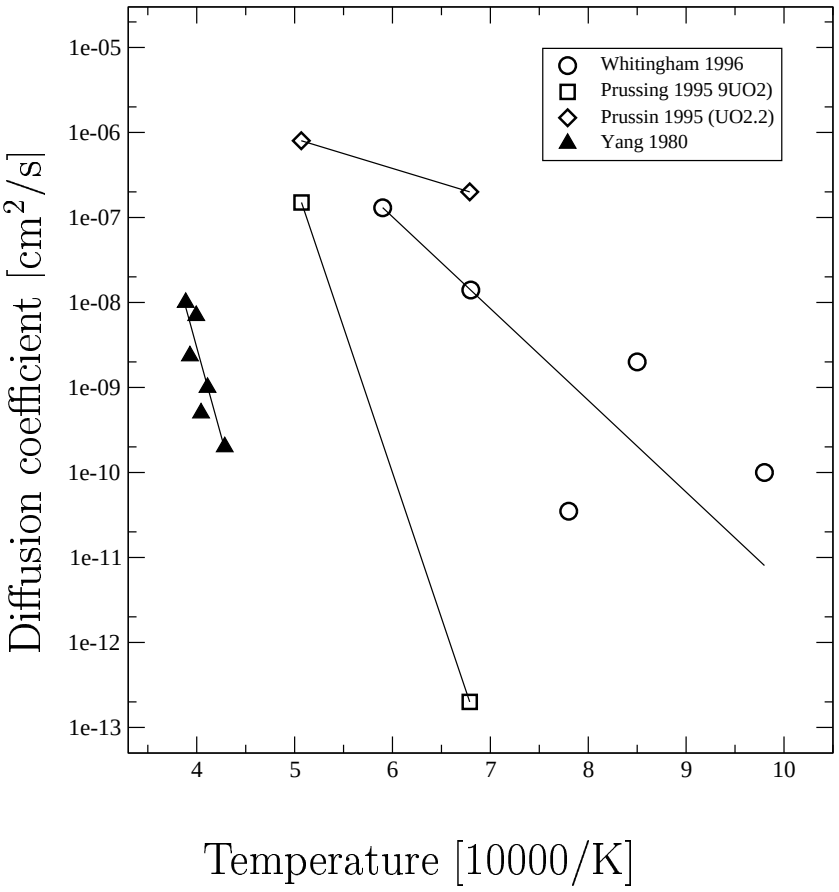

Figure 4.6: Diffusion of ruthenium in UO_2, $UO_{2.2}$ and U_3O_8. Only the results by Yang are true diffusion coefficients; all other data needs to be multiplied with the elusive Booth a^2 parameter.

4.2 U_3O_8

In the oxidation of UO_{2+x}, when x exceeds 2.25 and at temperatures greater than 1400K, a mixed phase of UO_2 and α'-U_3O_8 results. A pure form of the hexagonal, planar α'-U_3O_8 structure [89] (space group $P\bar{6}2m$, No. 189) is formed when the O/U ratio reaches 2.6. When UO_2 is oxidised to this phase, its structural properties change significantly and it becomes a powder.

Most studies on U_3O_8 are X-ray or neutron diffraction studies and as Table 4.6 clearly shows, there has been a lot of debate about the different types of U_3O_8 that may be formed. The only other important phase on the right hand side of the phase diagram is orthorombic α-U_3O_8, which is a low temperature phase of U_3O_8 (<1000K), which shows large similarity with the hexagonal structure.

In terms of defects and fission products the U_3O_8 phase has not been studied as extensively as the UO_2 phase. For example, there is no experimental data on the Schottky or Frenkel processes.

4.2.1 Self-diffusion in U_3O_8

Cation migration has been studied by Leme and Matzke [48], although their crystallographic data (compared to Loopstra [90]) suggests that it was not the expected hexagonal $\alpha'-U_3O_8$ phase they were investigating. Leme found an activation energy for uranium migration of 2.4eV by applying a thin layer of uranium-233 tracer and observing the penetration profile following different annealing steps.

Ball et al. [97, 99] have investigated the basic defect structures and migration behaviour (both interstitial and oxygen vacancy assisted) of small noble gas atoms neon, argon and the larger atoms krypton and xenon, via atomistic simulation.

Overview of relevant experimental U_3O_8 studies to date.	
Zachariasen, 1945 [91]	X-ray diffraction on low temperature form
Siegel, 1955	X-ray diffraction on high T (hexagonal) form
Hoekstra, 1955	The β-U_3O_8 structure
Andresen, 1958 [92]	Initial structure proposal for low T form
Chodura & Malý, 1958	Structure proposal for low T form
Loopstra, 1964 [89]	Better proposal for low T form
Loopstra 1969 [93]	Denial of existence of γ phase
Herak, 1969 [94]	Structure of high T form by X-ray & neutron
Rietveld, 1969	The Rietveld refinement method is published
Loopstra, 1970	Structure of the β-U_3O_8 phase
Loopstra, 1970 [90]	Phase transition orthogonal to hexagonal
Ackermann *et al.* , 1977	Thermal expansion and phase transitions
Glasser Leme & Matzke, 1983 [48]	Self-diffusion of uranium in U_3O_8
Naito *et al.* , 1983 [95]	Phase transitions and electrical conductivity
R. Williamson *et al.* , 1990 [87]	Importance of U_3O_8 in Ru release mechanism
Bradford 1996 [9]	Oxidation of urania in CO/CO_2
Whittingham *et al.* , 1996 [83]	Ruthenium behaviour

Table 4.6: Relevant experimental U_3O_8 studies to date.

Overview of relevant U_3O_8 simulation studies to date.	
Ball & Dickens, 1990 [96]	Proposal of a $U^{5\frac{1}{3}}$ model
Ball & Grimes, 1992 [97]	Behaviour of noble gasses Ne, Ar, Kr & Xe
Busker and Grimes, 1997 [98]	Behaviour of Caesium

Table 4.7: Relevant U_3O_8 simulation studies to date.